

This article was downloaded by: [Renmin University of China]

On: 13 October 2013, At: 11:06

Publisher: Taylor & Francis

Informa Ltd Registered in England and Wales Registered Number: 1072954 Registered office: Mortimer House, 37-41 Mortimer Street, London W1T 3JH, UK



Molecular Crystals and Liquid Crystals

Publication details, including instructions for authors and subscription information:

<http://www.tandfonline.com/loi/gmcl20>

Theoretical Studies on the Electronic Structures and Spectral Properties of Three Iridium(III) Complexes With Different N⁺N Ligands

Deming Han^a, Gang Zhang^b, Hongxing Cai^c, Xihe Zhang^c & Lihui Zhao^a

^a International Joint Research Center for Nanophotonics and Biophotonics, School of Life Science and Technology, Changchun University of Science and Technology, Changchun, Jilin, P. R. China

^b State Key Laboratory of Theoretical and Computational Chemistry, Institute of Theoretical Chemistry, Jilin University, Changchun, Jilin, P. R. China

^c International Joint Research Center for Nanophotonics and Biophotonics, School of Science, Changchun University of Science and Technology, Changchun, Jilin, P. R. China

Published online: 22 Apr 2013.

To cite this article: Deming Han, Gang Zhang, Hongxing Cai, Xihe Zhang & Lihui Zhao (2013) Theoretical Studies on the Electronic Structures and Spectral Properties of Three Iridium(III) Complexes With Different N⁺N Ligands, *Molecular Crystals and Liquid Crystals*, 575:1, 140-151, DOI: [10.1080/15421406.2013.766921](https://doi.org/10.1080/15421406.2013.766921)

To link to this article: <http://dx.doi.org/10.1080/15421406.2013.766921>

PLEASE SCROLL DOWN FOR ARTICLE

Taylor & Francis makes every effort to ensure the accuracy of all the information (the "Content") contained in the publications on our platform. However, Taylor & Francis, our agents, and our licensors make no representations or warranties whatsoever as to the accuracy, completeness, or suitability for any purpose of the Content. Any opinions and views expressed in this publication are the opinions and views of the authors, and are not the views of or endorsed by Taylor & Francis. The accuracy of the Content should not be relied upon and should be independently verified with primary sources of information. Taylor and Francis shall not be liable for any losses, actions, claims, proceedings, demands, costs, expenses, damages, and other liabilities whatsoever or howsoever caused arising directly or indirectly in connection with, in relation to or arising out of the use of the Content.

This article may be used for research, teaching, and private study purposes. Any substantial or systematic reproduction, redistribution, reselling, loan, sub-licensing, systematic supply, or distribution in any form to anyone is expressly forbidden. Terms & Conditions of access and use can be found at <http://www.tandfonline.com/page/terms-and-conditions>

Theoretical Studies on the Electronic Structures and Spectral Properties of Three Iridium(III) Complexes With Different N^N Ligands

DEMING HAN,¹ GANG ZHANG,² HONGXING CAI,³
XIHE ZHANG,³ AND LIHUI ZHAO^{1,*}

¹International Joint Research Center for Nanophotonics and Biophotonics, School of Life Science and Technology, Changchun University of Science and Technology, Changchun, Jilin, P. R. China

²State Key Laboratory of Theoretical and Computational Chemistry, Institute of Theoretical Chemistry, Jilin University, Changchun, Jilin, P. R. China

³International Joint Research Center for Nanophotonics and Biophotonics, School of Science, Changchun University of Science and Technology, Changchun, Jilin, P. R. China

*We report a quantum chemical study of the electronic structures and spectral properties of three iridium(III) biscarbene complexes with different heteroleptic N^N ligands. The theoretical calculation reveals that the lowest-lying singlet absorptions at 434 nm for **1** and 487 nm for **3** are attributed to the mixed transition characters of metal-to-ligand charge transfer (MLCT) and ligand-to-ligand charge transfer (LLCT). However, for **2**, the lowest-lying singlet absorption at 509 nm is attributed to the MLCT. For **1–3**, the phosphorescence at 739, 913, and 737 nm are mainly attributed to ³MLCT and ³LLCT characters. For **1** and **3**, the emission energies are nearly the same, which is larger than that of **2**. Ionization potentials (IP) and electron affinities (EA) calculations show that the assumed complex **3** has large EA value and enhanced electron injection ability as compared to complexes **1** and **2**. Moreover, the reasons for different transition characters and phosphorescence quantum yield for the three complexes have been discussed in this paper. This theoretical contribution allows the factors determining the efficiency of radiative and nonradiative decay pathways in the three complexes.*

Keywords Absorption; DFT; emission; iridium; phosphorescence

1. Introduction

In recent years, research on transition metal phosphorescent complexes is of great interest in designing of emissive dopants for phosphorescent organic light-emitting diodes (OLEDs) [1–7]. The use of transition metal ions such as Ru(II), Os(II), Ir(III), and Pt(II) in OLEDs is mainly due to their high phosphorescence emission quantum yields, short triplet excited state lifetime, and photochemical stability [8–10]. Thomas et al. [11] have studied a series

*Address correspondence to Lihui Zhao, International Joint Research Center for Nanophotonics and Biophotonics, School of Life Science and Technology, Changchun University of Science and Technology, Changchun 130022, Jilin, P. R. China. Tel.: +86-431-85583023; Fax: +86-431-85583099. E-mail: zhaohl@cust.edu.cn

of biscyclometalated Pt(II) complexes containing different electron-releasing groups that show strong phosphorescence at room temperature. Many phosphorescent transition metal complexes of Ir(III) [12], Ru(II) [13], and Os(II) [14] have been investigated by several research groups. Some rhenium(I) complexes with different ligands have been reported, and parts of them have been applied as emitters in OLEDs [15–19]. Their emissions have been attributed to the triplet metal-to-ligand charge transfer ($^3\text{MLCT}$) transitions in both theoretical studies and experiments [20–22]. In theory, internal phosphorescence quantum efficiency can be achieved as high as 100%, because $^3\text{MLCT}$ state can emit effectively by mixing the intensity of the spin-allowed metal-to-ligand charge-transfer (MLCT) state by strong spin-orbit coupling effects of the transition metal [23,24].

Nowadays, researchers pay a significant amount of efforts to the design and preparation of iridium(III)-based phosphorescent complexes because of their potential practical applications in OLEDs. These materials have high phosphorescent efficiencies, short lifetimes, and broad range of emission colors spanning the whole visible spectra. In the previous studies, most researchers relied on the modification of C,N-heteroaromatic (C^N) ligand for wide-range altering of the emission wavelength and color. For example, fac-Ir(ppy)₃ (fac-tris(2-phenylpyridine)iridium) [25] can give green light emission. In addition, the introduction of electron withdrawing or donating groups to the aryl ring or pyridine rings [26–28] is also an approach for tuning the emission energy. Indeed, the emission of the iridium complex can also be tuned by extending the π -conjugation of the ligand [29,30].

In this study, we propose two assumed structures (**2** and **3** in Fig. 1) on the basis of the experimental molecular structures of **1**. By using the density functional theory (DFT) and time-dependent density functional theory (TDDFT), the electronic structures, charge injection, and transport, and spectral properties of the three complexes have been calculated. This work provides a theoretical basis for future design and synthesis of new iridium complexes suited to phosphorescence emitter in electroluminescent layered structure.

2. Computational Details

The ground-state geometries were fully optimized by the density functional theory (DFT) based method Becke's LYP (B3LYP) exchange-correlation functional [31,32]. The excited-state geometries were optimized by the configuration interaction with the time-dependent density functional theory (TDDFT) method associated with the polarized continuum model (PCM) in dichloromethane (CH₂Cl₂) media [33]. In all calculations, the split valence 6–31G(d) basis set was adopted for the ligands and the LANL2DZ basis set was used for iridium(III). Both the absorption wave lengths and the emission wave lengths were calculated by time-dependent density functional theory (TDDFT) method based on the optimized ground-state structures at the B3LYP/6–31G(d)+LANL2DZ level and the lowest triplet excited-state structures at the TDDFT/B3LYP/6–31G(d)+LANL2DZ level [34,35]. All the calculations were performed with the Gaussian 09 software package [36].

3. Results and Discussion

3.1 Geometries in the Ground State

Two molecules [(mpmi)₂Ir(idiq)] (denoted as **2**) and [(mpmi)₂Ir(iqbi)] (denoted as **3**) have been theoretically designed based on the detailed analysis of electronic structure of the

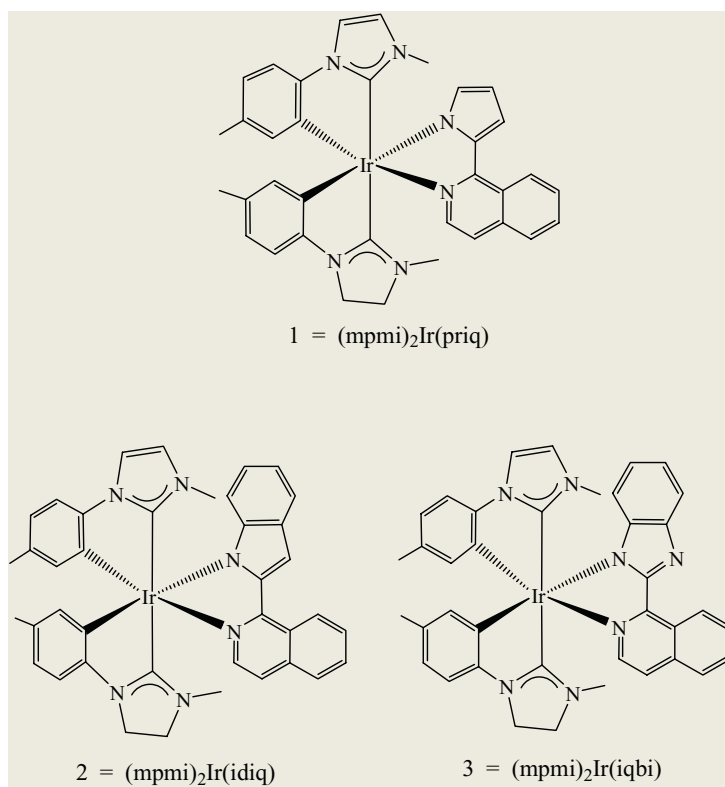


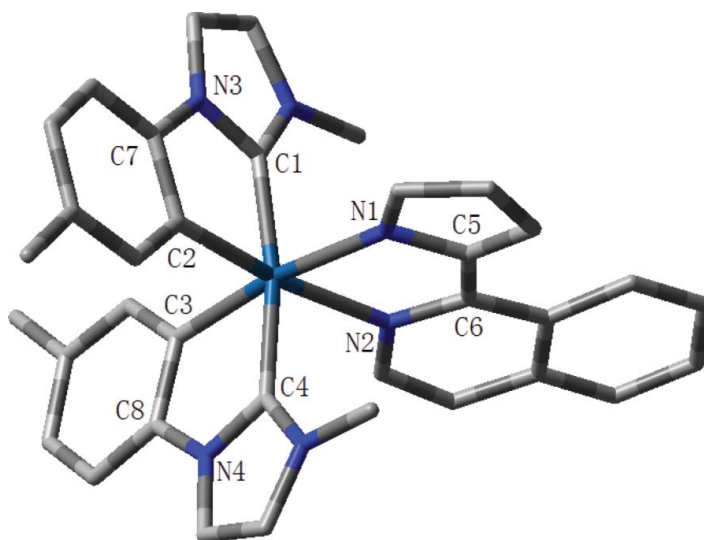
Figure 1. The schematic structures for the studied complexes **1–3**.

newly reported Iridium biscarbene complex [(mpmi)₂Ir(priq)] (denoted as **1**). It can be expected that the effect of extended π -conjugation is important to the electronic structures and spectral properties for these Iridium complexes. The schematic structures of the studied complexes **1–3** and the representative optimized structure of **3** in the ground state (S_0) at B3LYP level are shown in Figs 1 and 2, respectively. The optimized geometry parameters of **1–3** in the ground and lowest triplet states (T_1) together with the available single-crystal X-ray diffraction data of **1** are shown in Table 1. Figure 2 gives the atom label used in Table 1.

The calculated results reveal that all these heteroleptic iridium complexes possess a distorted octahedral configuration with the two carbene groups being trans to each other and the two 4-tolyl groups occupying the cis positions. Respectively, the complexes **1–3** can also be named as (mpmi)₂Ir(priq), (mpmi)₂Ir(idiq), and (mpmi)₂Ir(iqbi), where mpmi is the common carbene ligand and priq, idiq, and iqbi are the three N^{*}N ligands. These optimized bond distances of **1** agree well with the available experimental data [37], and the deviation is within 3%. Table 1 also shows that changes of the ligands have little influence on the metal-ligand (Ir–C and Ir–N) bond distances. For **1–3**, their ligands are nearly planar, indicating that they possess rigid skeletal structures, which may effectively prevent the nonradiative decay. In **1–3**, the bond angles of N1–Ir–N2, C1–Ir–C4, and C1–Ir–N1 are about 75°, 170°, and 90°. The dihedral angles N1–C5–C6–N2 of **1** and **2** are 7.99° and 10.46°, larger than that of **3**.

Table 1. Main optimized geometry parameters for **1–3** together with the experimental data of **1**

	1		2		3		Exp. ^a
	S ₀	T ₁	S ₀	T ₁	S ₀	T ₁	
Bond length(Å)							
Ir-C1	2.0538	2.0525	2.0571	2.0557	2.0581	2.0586	2.0155
Ir-C2	2.0515	2.0542	2.0527	2.0625	2.0518	2.0555	2.0217
Ir-C3	2.0611	2.0577	2.0580	2.0618	2.0581	2.0586	2.0592
Ir-C4	2.0566	2.0580	2.0574	2.0582	2.0534	2.0565	2.0535
Ir-N1	2.1468	2.1560	2.1763	2.1494	2.1636	2.1476	2.0995
Ir-N2	2.2063	2.1857	2.2064	2.1814	2.2177	2.1936	2.1537
C7-N3	1.4222	1.4229	1.4215	1.4230	1.4218	1.4224	1.4515
C8-N4	1.4241	1.4241	1.4238	1.4231	1.4242	1.4240	1.3963
C5-C6	1.4394	1.4193	1.4500	1.4191	1.4596	1.4108	1.4189
Bond angle(deg)							
N1-Ir-N2	75.01	75.32	74.81	75.56	74.59	75.76	76.16
C1-Ir-C4	170.68	170.82	170.72	169.56	170.71	171.07	168.04
C1-Ir-N1	90.38	89.70	90.11	90.98	89.71	89.87	92.42
Dihedral angle(deg)							
C1-N3-C7-C2	0.26	0.78	0.71	0.02	0.28	0.37	0.26
N1-C5-C6-N2	7.99	8.36	10.46	6.67	1.35	0.33	2.35
C3-C8-N4-C4	1.10	0.12	0.94	0.28	0.38	0.14	4.25

^aRef. [37].**Figure 2.** Representative optimized structure of **1** in the ground state.

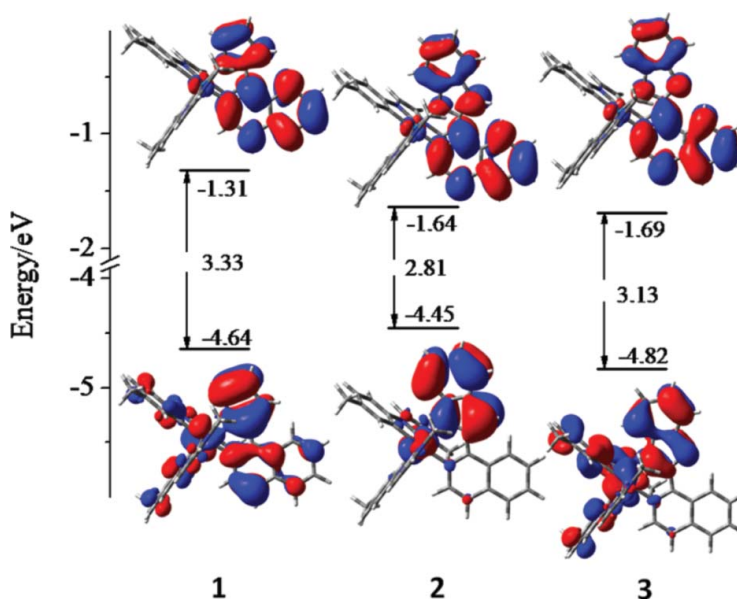


Figure 3. Energy levels and electron density plots of HOMO and LUMO for the studied complexes 1–3.

3.2 Frontier Molecular Orbital Properties

The properties of the excited states and electron transitions of organic light-emitting materials are closely related to the characters of the frontier molecular orbitals (FMO), especially HOMO (highest occupied molecular orbital) and LUMO (lowest unoccupied molecular orbital). We calculated the energy levels of FMO and energy gaps between of LUMO and HOMO (ΔE_{L-H}) for 1–3. The HOMO and LUMO distribution, energy levels, and energy gaps are plotted in Fig. 3. The calculated FMO compositions for 1–3 were also listed in Tables S1–S3 (Supplemental material, available online only).

For **1**, the HOMO lying at -4.64 eV is composed of 13% Ir d-orbital and 73% π -orbital of priq ligand. The LUMO of **1** lying at -1.31 eV is mainly composed of 97% antibonding π^* of priq ligand. For **2**, the HOMO lying at -4.45 eV is composed of 83% Ir d-orbital and 13% π -orbital of idiq ligand. The LUMO of **2** lying at -1.64 eV is mainly composed of 97% antibonding π^* of idiq ligand. Compared to that of **1**, the raised HOMO energy level of **2** owing to the effect of extended π -conjugation will benefit the hole-transporting ability. For **3**, the HOMO lying at -4.82 eV is composed of 32% Ir d-orbital, 37% π -orbital of priq ligand, and 31% mpmi ligand. The LUMO of **3** lying at -1.69 eV is mainly composed of 97% antibonding π^* of iqbi ligand. In addition, the HOMO-LUMO energy gaps are 3.33 eV for **1**, 2.81 eV for **2**, 3.13 eV for **3**, respectively. It can be seen that the ΔE_{L-H} of the assumed **2** and **3** are smaller than that of **1** owing to the effect of extended π -conjugation. It is obvious in Fig. 3 that the distribution of the electron cloud of HOMO for **2** and **3** complexes is different from that of **1**. However, the electron cloud of LUMO for these complexes has the similar distributions. The main reason resulting in this different distribution from **2** and **3** is due to the effect of extended π -conjugation by the introduction of phenyl ring substituent. With respect to **1** and **2**, the lower HOMO and LUMO energy levels of **3** will ensure the efficient hole injection abilities and the electron injection abilities,

Table 2. Ionization potentials, electron affinities, extraction potentials, and internal reorganization energies for complexes **1–3** (eV)

	IP (v)	IP (a)	EA (v)	EA (a)	HEP	EEP	λ_{hole}	$\lambda_{\text{electron}}$
1	5.78	5.69	0.03	0.14	5.62	0.31	0.16	0.33
2	5.65	5.49	0.38	0.51	5.33	0.65	0.31	0.26
3	5.92	5.80	0.43	0.57	5.67	0.72	0.24	0.29

respectively. These relative HOMO and LUMO energy levels will guide to compare the electroluminescent (EL) efficiency of OLEDs among these complexes.

3.3 Ionization Potentials (IP) and Electronic Affinities (EA)

Ionization potential (IP), electron affinity (EA), and migration of charge are three key factors for designing OLEDs materials. EA and IP, which are closely related to HOMO and LUMO, respectively, are used to evaluate charge injection abilities of luminescent materials. A larger EA (smaller IP) indicates easier injection of electrons (holes) into the emitting materials from the electron (hole) transporting layer. The reorganization energy (λ) can evaluate the charge transfer rate and balance. The calculated IP, EA, and λ , together with HEP (hole extraction potential, the energy difference between M (neutral molecule) and M⁺ (cationic), using the M⁺ geometry) and EEP (electron extraction potential, the energy difference between M and M⁻ (anionic), using M⁻ geometry) values are listed in Table 2. It can be seen that the calculated IP (both vertical and adiabatic) values increase in the following order: **2** < **1** < **3**. This indicates that the difficulties of hole injection from hole-transport layer to these complexes gradually increase. A larger EA (smaller IP) suggests that it is easier to inject electrons (holes) into the emitting materials from the electron (hole) transporting layer. Complex **2** has the smallest IP value, which is consistent with its highest HOMO energy level, and thus its hole injection is the easiest. Corresponding to the lowest LUMO energy level, the assumed complex **3** has large EA value and enhanced electron injection ability as compared to complexes **1** and **2**.

According to the Marcus/Hush model [38–40], the charge (hole or electron) transfer rate k can be expressed by the following formula:

$$k = \left(\frac{\pi}{\lambda k_{\text{b}} T} \right)^{1/2} \frac{V^2}{h} \exp \left(-\frac{\lambda}{4k_{\text{b}} T} \right) = A \exp \left(-\frac{\lambda}{4k_{\text{b}} T} \right) \quad (1)$$

where T is the temperature, k_{b} is the Boltzmann constant, λ is the reorganization energy, and V is the coupling matrix element between the ions and molecules, which is dictated by the overlap of orbitals. Due to the limited intermolecular charge transfer range in solid state, the mobility of charges dominantly relates to the reorganization energy λ for OLEDs materials. Therefore, a low λ value is required for an efficient charge transport process.

The reorganization energy λ (herein the internal reorganization energy obtained by ignoring any environmental relaxation and changes) for hole transfers can be expressed as follows [41]:

$$\lambda_{\text{hole}} = \lambda_0 + \lambda_{+} = (E_0^* - E_0) + (E_0^* - E_{+}) = \text{IP}_{(\text{v})} - \text{HEP} \quad (2)$$

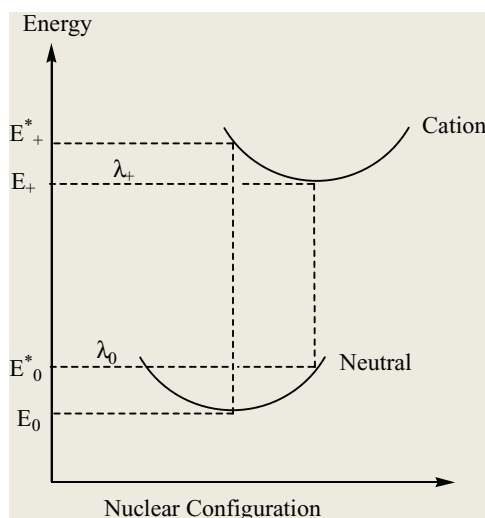


Figure 4. Schematic description of internal reorganization energy for hole transfer.

As illustrated in Fig. 4, E_0 and E_+ represent the energies of the neutral and cationic species in their lowest energy geometries, respectively, while E_0^* and E_+^* represent the energies of the neutral and cationic species with the geometries of the cationic and neutral species, respectively, which is equal to the difference between vertical IP and hole extraction energy HEP. In this way, λ for electron transfer can also be expressed similar to that for hole transfer:

$$\lambda_{\text{electron}} = \text{EEP} - \text{EA}(\text{v}) \quad (3)$$

According to Eqs. (2) and (3), we calculated the λ_{hole} and $\lambda_{\text{electron}}$ of these studied complexes. Table 2 shows that the reorganization energies for electron transport ($\lambda_{\text{electron}}$) are larger than those for hole transport (λ_{hole}) except for **2**, which reveals that the hole-transport performance of these complexes is better than electron-transporting performance. The differences between λ_{hole} and $\lambda_{\text{electron}}$ for **2** and **3** are small, so hole and electron transfer balance could be achieved easily in emitting layer, which is the key factor for efficient OLEDs materials. Moreover, the $\lambda_{\text{electron}}$ values of the assumed complexes **2** and **3** are smaller than that of complexes **1**, leading to the easier electron transfer for **2** and **3**.

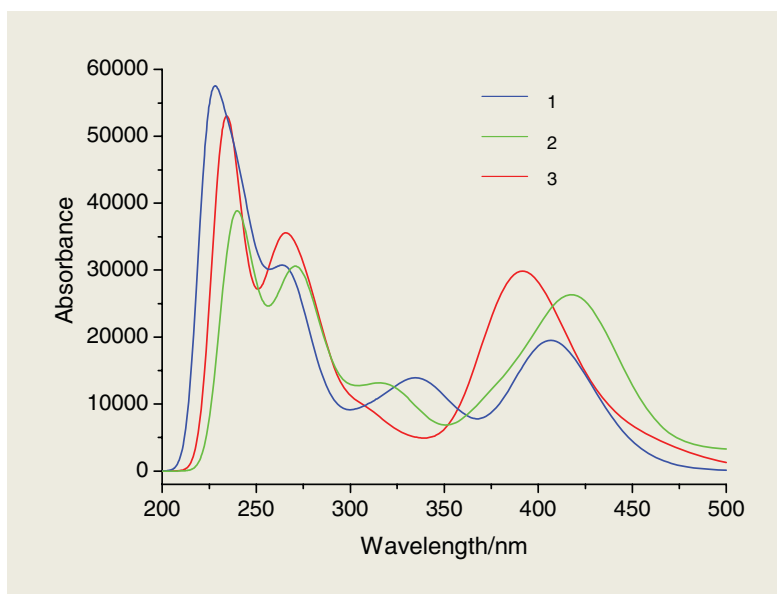
3.4 Absorption Spectra

The absorption spectra in CH_2Cl_2 solution for **1–3** were studied at the TDDFT/B3LYP level. The polarized continuum model (PCM) in self-consistent reaction field (SCRF) is used in which the solvent is simulated as a continuum of uniform dielectric constant ϵ . The calculated absorption spectra associated with their oscillator strengths (f), assignment, configurations, and excitation energies are listed in Table 3. Simulated UV-visible absorption spectra for **1–3** have been depicted in Fig. 5.

As shown in Table 3, the lowest lying singlet \rightarrow singlet absorption of **1–3** are located at 434, 509, and 487 nm, respectively. It can be seen that the calculated 434 nm absorption for **1** is comparable with the experimental value of 420 nm [37]. The lowest lying singlet \rightarrow singlet absorptions of **2** and **3** are red-shifted compare to that of **1**, which is consistent

Table 3. Selected calculated wavelength (nm)/energies (eV), oscillator strength (f), major contribution, transition characters, and the available experimental absorption wavelength (nm) for **1–3** in CH₂Cl₂ media

	State	λ /E	f	Configuration	Nature	Exp. ^a
1	S ₁	434/2.85	0.0190	H→L(54%) H-1→L(44%)	MLCT/LLCT MLCT/LLCT	420
	S ₂	408/3.04	0.1962	H→L(31%) H-1→L(46%)	MLCT/LLCT MLCT/LLCT	
	S ₅	340/3.64	0.0840	H→L+1(81%)	MLCT	324
	S ₂₁	274/4.51	0.0701	H-3→L+2(72%)	MLCT/LLCT/ILCT	272
	S ₁₁	323/3.84	0.0833	H-2→L+1(80%)	MLCT/LLCT	
2	S ₁	509/2.43	0.0344	H→L(96%)	MLCT	
	S ₃	420/2.94	0.3325	H-2→L(91%)	MLCT	
	S ₅	375/3.31	0.0844	H-4→L(90%)	MLCT/LLCT	
	S ₁₁	323/3.84	0.0833	H-2→L+1(80%)	MLCT/LLCT	
3	S ₁	487/2.54	0.0056	H→L(98%)	MLCT/LLCT	
	S ₃	407/3.04	0.1670	H-2→L(81%)	MLCT	
	S ₇	336/3.68	0.0171	H→L+1 (96%)	MLCT/LLCT	
	S ₁₀	320/3.86	0.0143	H→L+2(82%)	MLCT/LLCT/ILCT	
	S ₂₈	265/4.67	0.1407	H-5→L+1(50%)	MLCT/LLCT	

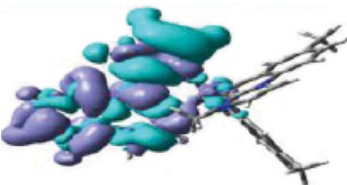
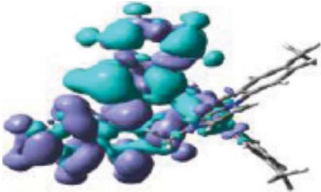
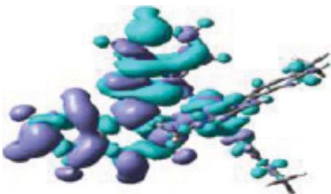
^aRef. [37].**Figure 5.** Simulated absorption spectra in CH₂Cl₂ media for complexes **1–3**.

with the variation rules of the ΔE_{L-H} values. The configurations of HOMO \rightarrow LUMO are responsible for the lowest lying transitions of the three complexes, especially for **2** and **3**, which mostly originate from a HOMO \rightarrow LUMO transition. In Fig. 5, the first distinguished absorption bands appear at 220–275 nm. For the three complexes, the transitions with the largest oscillator strengths located at around 223 nm dominate these higher-energy absorption bands. The second weaker bands appear at the visible region (400–500 nm). For **1** and **3**, the lowest lying absorptions can be characterized as MLCT (metal to ligand charge transfer)/LLCT (ligand-to-ligand charge transfer), with the exception of **2**, which is mainly the transition with MLCT character.

3.5 Phosphorescence Spectra

The lowest lying triplet excited state geometries of **1–3** are optimized based on the calculated ground state geometries and selected geometrical parameters are also listed in Table 1. From S_0 to T_1 states, the bond angles of N1–Ir–N2, C1–Ir–C4, and C1–Ir–N1 are slightly changed. The dihedral angles of C3–C8–N4–C4 become smaller from S_0 to T_1 state. On the basis of the optimized T_1 structures, the emission wavelengths, emission energies, and transition nature were calculated by the TDDFT method listed in Table 4. For comparison, the available experimental values are also listed. The calculated emission energies for **1** (1.67 eV, 739 nm) is smaller as compared to the corresponding experimental value 599 nm

Table 4. Calculated emission energies of T_1 and their transition nature for complexes **1–3** in CH_2Cl_2 media, as well as the available experimental wavelengths (nm)

$\lambda(\text{nm})/E(\text{eV})$	Nature ^a	Exp. ^b
1 T_1 739/1.67	 ³ LMCT	599
2 T_1 913/1.35	 ³ LMCT	
3 T_1 737/1.68	 ³ LMCT/ ³ LLCT	

^aChange of electron density distribution upon the $T_1 \rightarrow S_0$ transition for complexes **1–3**. Cyan and violet colors represent the decrease and increase of electron density, respectively.

^bRef. [37].

[37]. The emission energy of **2** (1.35 eV) is red-shifted as compared to that of **1** (1.67 eV), but their luminescent nature is nearly the same, that is, ligand to metal charge transfer. In addition, **2** has the same phosphorescent characters to **1**, that is, one ligand to metal charge transfer. The emission energy of **3** (1.68 eV) is similar to that of complex **1** with the different luminescent nature, that is, ³LMCT/³LLCT.

The emission quantum yield (Φ) from an emissive excited state to the ground state is generally formulated as:

$$\Phi = k_r / (k_r + k_{nr}), \quad (4)$$

where k_r and k_{nr} are radiative and nonradiative rate constants, respectively. Thus, for obtaining an efficient phosphorescent material, a large k_r and a small k_{nr} are required. The rate constants depend strongly on the energy of lowest triplet excited state (E_{T_1}) for phosphorescence, expressed as:

$$k_{nr} = \alpha \exp(-\beta E_{T_1}), \quad (5)$$

$$k_r = \gamma (E_{T_1})^3 |M_{T-S}|^2, \quad (6)$$

where α , β , and γ are constant; $|M_{T-S}|$ is the emission transition moment from the triplet state. Eq. (5) is well-known as “the energy gap law” [42], which indicates that k_{nr} decreases with the increase of E_{T_1} . On the contrary, Eq. (6) shows that k_r increases with the increase of E_{T_1} . Thus, a large E_{T_1} is essential for an efficient material. Table 4 indicates that **3** has the largest E_{T_1} followed by **1** and **2** in CH₂Cl₂ media. Hence, the assumed complex **3** is a good candidate to be an efficient phosphorescent material.

The presence of a heavy atom, such as iridium, is anticipated to increase the spin-orbit coupling (SOC) and thus intersystem crossing (ISC), on the condition that its orbitals make a significant contribution in the excited states involved. Thus, the SOC effects are elucidated mainly from the following two aspects. One is the contribution of ³MLCT in the T_1 state [43]. The direct involvement of the d(Ir) orbital enhances the first-order SOC in the $T_1 \rightarrow S_0$ transition, which would result in a drastic decrease of the radiative lifetime and avoid the nonradiative process [44]. Thus, a large ³MLCT contribution facilitates the increase of the quantum yield. In Table 5, we list the ³MLCT contributions, which were calculated to be 10.12%, 10.02%, and 20.88% for **1**, **2**, and **3**, respectively. We noted that for **3** the 20.88% of ³MLCT is higher than those of **1** and **2**. The second aspect elucidating the SOC effects is the S_1 - T_1 energy gap (ΔE_{ST}) [45]. The $S_1 \rightarrow T_1$ ISC induced by SOC interactions of the triplet state with the singlet state plays an important role in the phosphorescent process. Thus, a minimal ΔE_{ST} is required for enhancing the ISC rate, leading to the increased k_r . Seen from the Table 5, the calculated results for ΔE_{ST} are 0.93, 0.70, and 0.58 eV for **1**, **2**, and **3**, respectively. The complex **3** has smaller ΔE_{ST} value than that of **1** and **2**.

Table 5. Contribution of ³MLCT in the T_1 state and values of the $S_1 \rightarrow T_1$ energy gaps (ΔE_{ST}) for complexes **1–3**

	³ MLCT(%)	ΔE_{ST} (eV)
1	10.12	0.93
2	10.02	0.70
3	20.88	0.58

From the discussion above, it can be seen that the radiative decay rate constants (k_r) are related to many factors. Evidently, a larger MLCT contribution and lower S_1 - T_1 energy gap (ΔE_{ST}) may account for a larger k_r according to Eq. (6). Besides the factors mentioned above, other factors may also play an important role for a high quantum yield, because Φ is the competition between k_r and k_{nr} (Eq. (4)).

4. Conclusions

In this article, we have reported the detail investigation of geometrical structures, transporting abilities, absorptions, and phosphorescent properties for three heteroleptic iridium(III) biscarbene complexes. The calculated results demonstrated that the heteroleptic N^N ligands play a very important role for the control of the emission. The lowest lying singlet absorptions at 434 nm for **1** and 487 nm for **3** are attributed to the mixed transition characters of MLCT and LLCT. For **2**, the lowest lying singlet absorption at 509 nm is attributed to the MLCT. The calculated phosphorescence at 739, 913, and 737 nm is mainly attributed to $^3\text{MLCT}$ and $^3\text{LLCT}$ characters. **1** and **3** have the nearly same emission energies and larger than that of **2**. The calculated ionization potentials (IP), electron affinities (EA), and reorganization energy (λ) indicate that **3** has the higher efficiency of OLEDs than that of **1** and **2**. We hope that this theoretical work can provide a suitable guide to the future design and synthesis of novel phosphorescent materials for use in the OLEDs.

Acknowledgments

The authors are grateful for the financial aid from the Program of Science and Technology Development Plan of Jilin Province (Grant No. 20110438) and the Funds for Doctoral Scientific Research Startup of Changchun University of Science and Technology (Grant No. 40301855).

References

- [1] Yu, X. M., Kwok, H. S., Wong, W. Y., & Zhou, G. J. (2006). *Chem. Mater.*, *18*, 5097.
- [2] Bolink, H. J., Coronado, E., Santamaria, S. G., Sessolo, M., Evans, N., Klein, C., Baranoff, E., Kalyanasundaram, K., Graetzel, M., & Nazeeruddin, M. K. (2007). *Chem. Commun.*, *31*, 3276.
- [3] Park, G. Y., & Ha, Y. (2008). *Synthetic Met.*, *158*, 120.
- [4] Lee, T. C., Hung, J. Y., Chi, Y., Cheng, Y. M., Lee, G. H., Chou, P. T., Chen, C. C., Chang, C. H., & Wu, C. C. (2009). *Adv. Funct. Mater.*, *19*, 2639.
- [5] Che, C. M., Kwok, C. C., Lai, S. W., Rausch, A. F., Finkenzeller, W. J., Zhu, N. Y., & Yersin, H. (2010). *Chem. Eur. J.*, *16*, 233.
- [6] Tao, S. L., Lai, S. L., Wu, C. A., Ng, T. W., Chan, M. Y., Zhao, W. M., & Zhang, X. H. (2011). *Org. Electron.*, *12*, 2061.
- [7] Kim, D., Zhu, L. Y., & Brédas, J. L. (2012). *Chem. Mater.*, *24*, 2604.
- [8] Costa, B. D., Céspedes-Guirao, F. J., Ortí, E., Bolink, H. J., Gierschner, J., Fernández-Lázaro, F., & Sastre-Santos, A. (2009). *Chem. Commun.*, *26*, 3886.
- [9] Tamayo, A. B., Garon, S., Sajoto, T., Djurovich, P. I., Tsyba, I. M., Bau, R., & Thompson, M. E. (2005). *Inorg. Chem.*, *44*, 8723.
- [10] Lowry, M. S., Hudson, W. R., Pascal, R. A., & Bernhard, S. (2004). *J. Am. Chem. Soc.*, *126*, 14129.
- [11] Thomas, S., Venkatesan, K., Müller, P., & Swager, T. M. (2006). *J. Am. Chem. Soc.*, *128*, 16641.
- [12] Whittle, V. L., & Williams, J. A. G. (2008). *Inorg. Chem.*, *47*, 6596.
- [13] Welter, S., Brunner, K., Hofstraal, J. W., & De Cola, L. (2003). *Nature*, *421*, 54.

- [14] Hsu, F. C., Tung, Y. L., Chi, Y., Hsu, C. C., Cheng, Y. M., Ho, M. L., Chou, P. T., Peng, S. M., & Carty, A. J. (2006). *Inorg. Chem.*, **45**, 10188.
- [15] Si, Z. J., Li, J., Li, B., Zhao, F. F., Liu, S. Y., & Li, W. L. (2007). *Inorg. Chem.*, **46**, 6155.
- [16] Li, X., Zhang, D. Y., Li, W. L., Chu, B., Han, L. L., Zhu, J. Z., Su, Z. S., Bi, D. F., Wang, D., Yang, D. F., & Chen, Y. R. (2008). *Appl. Phys. Lett.*, **92**, 083302.
- [17] Horvath, R., Otter, C. A., Gordon, K. C., Brodie, A. M., & Ainscough, E. W. (2010). *Inorg. Chem.*, **49**, 4073.
- [18] Fraser, M. G., Blackman, A. G., Irwin, G. I. S., Easton, C. P., & Gordon, K. C. (2010). *Inorg. Chem.*, **49**, 5180.
- [19] Werrett, M. V., Chartrand, D., Gale, J. D., Hanan, G. S., Maclellan, J. G., Massi, M., Muzzioli, S., Raiteri, P., Skelton, B. W., Silberstein, M., & Stagni, S. (2011). *Inorg. Chem.*, **50**, 1229.
- [20] Fang, Y. Q., Taylor, N. J., Hanan, G. S., Loiseau, F., Passalacqua, R., Campagna, S., Nierengarten, H., & Dorselaer, A. V. (2002). *J. Am. Chem. Soc.*, **124**, 7912.
- [21] Yam, V. W. W., Wong, K. M. C., Chong, S. H. F., Lau, V. C. Y., Lam, S. C. F., Zhang, L. J., & Cheung, K. K. (2003). *J. Organomet. Chem.*, **670**, 205.
- [22] Ma, Y. G., Zhang, H. X., Shen, J. C., & Che, C. M. (1998). *Synthetic Met.*, **94**, 245.
- [23] Adachi, C., Baldo, M. A., Forrest, S. R., & Thompson, M. E. (2000). *Appl. Phys. Lett.*, **77**, 904.
- [24] Harriman, A., & Izzet, J. (2007). *Phys. Chem. Chem. Phys.*, **9**, 944.
- [25] King, K. A., Spellane, P. J., & Watts, R. J. (1985). *J. Am. Chem. Soc.*, **107**, 1431.
- [26] Zhou, G., Ho, C. L., Wong, W. Y., Wang, Q., Ma, D., Wang, L., Lin, Z., Marder, T. B., & Beeby, A. (2008). *Adv. Funct. Mater.*, **18**, 499.
- [27] Ho, C. L., Wang, Q., Lam, C. S., Wong, W. Y., Ma, D., Wang, L., Gao, Z. Q., Chen, C. H., Cheah, K. W., & Lin, Z. (2009). *Chem. Asian. J.*, **4**, 89.
- [28] Zhou, G., Wang, Q., Wang, X., Ho, C. L., Wong, W. Y., Ma, D., Wang, L., & Lin, Z. (2010). *J. Mater. Chem.*, **20**, 7472.
- [29] Okada, S., Iwakaki, H., Furugori, M., Kamatain, J., Igawa, S., Moriyama, T., Miura, S., Tsuboyama, A., Takiguchi, T., & Mizutani, H. (2002). *Proceedings of SID'02*, Boston, USA, 1360.
- [30] Tsuboyama, A., Iwakaki, H., Furugori, M., Mukaide, T., Kamatani, J., Igawa, S., Moriyama, T., Miura, S., Takiguchi, T., Okada, S., Hoshino, M., & Ueno, K. (2003). *J. Am. Chem. Soc.*, **125**, 12971.
- [31] Runge, E., & Gross, E. K. U. (1984). *Phys. Rev. Lett.*, **52**, 997.
- [32] Mayo, S. L., Olafson, B. D., & Goddard, W. A. (1990). *J. Phys. Chem.*, **94**, 8897.
- [33] Mennucci, B., & Tomasi, J. (1997). *J. Chem. Phys.*, **106**, 5151.
- [34] Bak, K. L., Jørgensen, P., Helgaker, T., Rund, K., & Jensen, H. J. A. (1993). *J. Chem. Phys.*, **98**, 8873.
- [35] Autschbach, J., Ziegler, T., Gisbergen, S. J. A., & Baerends, E. J. (2002). *J. Chem. Phys.*, **116**, 6930.
- [36] Frisch, M. J. *et al.* (2009). *Gaussian 09*, Gaussian, Inc.: Wallingford, CT.
- [37] Lu, K. Y., Chou, H. H., Hsieh, C. H., Ou Yang, Y. H., Tsai, H. R., Tsai, H. Y., Hsu, L. C., Chen, C. Y., Chen, I. C., & Cheng, C. H. (2011). *Adv. Mater.*, **23**, 4933.
- [38] Marcus, R. A. (1956). *J. Chem. Phys.*, **24**, 966.
- [39] Marcus, R. A. (1993). *Rev. Mod. Phys.*, **65**, 599.
- [40] Hush, N. S. (1958). *J. Chem. Phys.*, **28**, 962.
- [41] Hutchison, G. R., Ratner, M. A., & Marks, T. J. (2005). *J. Am. Chem. Soc.*, **127**, 2339.
- [42] Wilson, J. S., Chawdhury, N., Al-Mandhary, M. R. A., Younus, M., Khan, M. S., Raithby, P. R., Köhler, A., & Friend, R. H. (2001). *J. Am. Chem. Soc.*, **123**, 9412.
- [43] Li, J., Djurovich, P. I., Alleyne, B. D., Yousufuddin, M., Ho, N. N., Thomas, J. C., Peters, J. C., Bau, R., & Thompson, M. E. (2005). *Inorg. Chem.*, **44**, 1713.
- [44] Yang, C. H., Cheng, Y. M., Chi, Y., Hsu, C. J., Fang, F. C., Wong, K. T., Chou, P. T., Chang, C. H., Tsai, M. H., & Wu, C. C. (2007). *Angew. Chem. Int. Ed.*, **46**, 2418.
- [45] Avilov, I., Minoofar, P., Cornil, J., & De Cola, L. (2007). *J. Am. Chem. Soc.*, **129**, 8247.